THE METHYLAZOXYMETHANOL ACETATE (MAM-E17) RAT MODEL: MOLECULAR AND FUNCTIONAL EFFECTS IN THE HIPPOCAMPUS

Eva Hradetzky, Thomas M. Sanderson, Tsz Tsang, John L. Sherwood, Stephen M. Fitzjohn, Viktor Lakics, Nadia Malik, Stephanie Schoeffmann, Michael F. O'Neill, Tammy M. K. Cheng, et al.

THE METHYLAZOXYMETHANOL ACETATE (MAM-E17) RAT MODEL: MOLECULAR AND FUNCTIONAL EFFECTS IN THE HIPPOCAMPUS

Eva Hradetzky[1,2], Thomas M. Sanderson[2], Tsz M. Tsang[3], John L. Sherwood[2], Stephen M. Fitzjohn[2], Viktor Lakics[2], Nadia Malik[2], Stephanie Schoeffmann[1], Michael J. O'Neill[2], Tammy M. K. Cheng[1], Laura W. Harris[1], Hassan Rahmoune[1], Paul C. Guest[1], Emanuele Sher[2], Graham L. Collingridge[4], Elaine Holmes[3], Mark D. Tricklebank [2*] and Sabine Bahn [1,5*]

*senior corresponding authors: sb209@cam.ac.uk, tricklebank_mark@lilly.com

[1]Department of Chemical Engineering and Biotechnology, University of Cambridge, Tennis Court Road, Cambridge, UK. [2]Lilly Centre for Cognitive Neuroscience, Eli Lilly & Co. Ltd., Erl Wood Manor, Windlesham, Surrey, UK. [3]Department of Biomolecular Medicine, Division of Surgery, Oncology, Reproductive Biology and Anesthetics, Faculty of Medicine, Imperial College, London, UK. [4]MRC Centre for Synaptic Plasticity, Department of Anatomy, School of Medical Sciences, University of Bristol, Bristol, UK. [5]Department of Neuroscience, Erasmus University Medical Centre, Rotterdam, NL

To whom correspondence may be addressed

Sabine Bahn, Ph.: +44 1223 334151; Fax: +44 1223 334162; Email address: sb209@cam.ac.uk

Running title

Molecular and functional effects in the MAM-E17 rat hippocampus

Keywords

Animal models, Schizophrenia, Biological Psychiatry, Signal Transduction, Methylazoxymethanol acetate, MAM, Hippocampus, Molecular screening, Electrophysiology, Mass spectrometry

Abbreviations

^{1}H-NMR- Proton nuclear magnetic resonance spectroscopy,

aCSF- Artificial cerebrospinal fluid,

AMPA- Alpha-amino-3-hydroxy-5-methyl-4-isoxazolepropionic acid,

AP5- 2-amino-5-phosphonopentanoic acid,

C18- Alkyl chain consisting of 18 carbons,

CA1- Cornu ammonis 1 of hippocampus,

CA3- Cornu ammonis 3 of hippocampus,

E17- Embryonic day 17,

fEPSP- Field excitatory post-synaptic potential,

FDR- False discovery rate,

FV- Fibre volley,

GABA- Gamma-aminobutyric acid,

GCPII- Glutamate carboxypeptidase II,

ID- Identification,

IPA- Ingenuity pathway analysis,

kPCA- Kernel principal component analysis,

MAM- Methylazoxymethanol acetate,

NAA- N-acetyl aspartate,

NAAG- N-acetyl aspartyl glutamate,

NMDA- N-methyl-D –aspartate,

NOESY- Nuclear Overhauser effect spectroscopy,

IPA- Ingenuity Pathway Analysis,

LC-MS^E- Liquid chromatography mass spectrometry in expression mode,

OPLS-DA- Orthogonal-projection on latent structures discriminant analysis,

p- P-value of a statistical significance test,

PC- Phosphocholine,

PCA- Principal component analysis,

PLS-DA- Partial least squares discriminate analysis,

PP- Protein phosphatase,

ppm- Parts per million,

q- Q-value,

SEM- Standard error of mean,

RD- Relaxation delay,

RSD- Relative standard deviation,

SD- Standard deviation,

TAC- Targeted analyte cluster,

TR- Repetition time

ABSTRACT

Administration of the DNA-alkylating agent methylazoxymethanol acetate (MAM) on embryonic day 17 (E17) produces behavioral and anatomical brain abnormalities which model some aspects of schizophrenia. This has lead to the premise that MAM rats are a neurodevelopmental model for schizophrenia. However, the underlying molecular pathways affected in this model have not been elucidated. In the present study, we investigated the molecular phenotype of adult MAM rats by focusing on the frontal cortex and hippocampal areas, as these are known to be affected in schizophrenia. Proteomic and metabonomic analyses showed that the MAM-treatment on E17 resulted primarily in deficits in hippocampal glutamatergic neurotransmission, as seen in some schizophrenia patients. Most importantly, these results were consistent with our finding of functional deficits in glutamatergic neurotransmission as identified using electrophysiological recordings. Thus, this study provides the first molecular evidence, combined with functional validation, that the MAM-E17 rat model reproduces hippocampal deficits relevant to the pathology of schizophrenia.

INTRODUCTION

Administration of the short-acting DNA-alkylating agent methylazoxymethanol acetate (MAM) (Cattabeni and Di Luca, 1997; Cattaneo et al, 1995; Meyn and Murray, 1984) on embryonic day 17 (E17) to rat dams interferes with the development of specific brain regions in the offspring (Bayer et al, 1993; Moore et al, 2006). Through selective disturbance of proliferation and migration of neuronal precursor cells undergoing their final mitosis, MAM induces morphological and cytological alterations modeling phenomena seen in schizophrenia *post mortem* brains (for review see Lodge and Grace, 2009b). Behavioral studies of offspring of MAM-treated rats (hereafter referred to as MAM rats) showed deficits in sensorimotor gating (Le Pen *et al*, 2006), an inability to ignore irrelevant stimuli (Flagstad *et al*, 2005), hypersensitivity to amphetamine and N-methyl-D-aspartate (NMDA) receptor antagonists (Penschuck *et al*, 2006), and social withdrawal (Flagstad *et al*, 2004) with onset in adolescence (Le Pen *et al*, 2006). Although direct evaluation of schizophrenia symptoms in animal models is inherently difficult, such effects have been related to neuropsychiatric deficits seen in schizophrenia (Braff *et al*, 1992; Hansen *et al*, 2009; Laruelle *et al*, 1996; Lubow and Gewirtz, 1995). Consequently, the MAM-E17 rat

model is widely thought to represent a neurodevelopmental model of schizophrenia (Lodge and Grace, 2009b).

Utilization of any model for investigation of pathological mechanisms and novel drug discovery requires identification of which molecular components of a disease can be represented. Apart from studies which have used immunohistochemical staining for parvalbumin and reelin in the frontal cortex and hippocampus (Lodge *et al*, 2009a; Matricon *et al*, 2010; Penschuck *et al*, 2006), molecular characterization of the MAM-E17 rat model has not yet been reported. Since most *post mortem* and *in vivo* studies of schizophrenia patients have identified deficits in the prefrontal cortex and hippocampus (Bertolino *et al*, 1996; Harrison, 1999; Tsai *et al*, 1995), we have attempted to identify expression differences in the proteome and metabonome of the equivalent brain regions in MAM rats. Furthermore, we evaluated if the identified molecular changes translate into synaptic physiology. Such analyses may provide molecular and physiological correlates for some of the histological and behavioral deficits seen in MAM rats. The relevance of these findings to schizophrenia is discussed.

MATERIAL AND METHODS

Animals

All procedures were conducted in full compliance with the Home Office Guidance (UK Animals Scientific Procedures Act 1986) and the ethical policies of Eli Lilly & Co. Sprague Dawley rat dams (Charles River; Margate, UK) were injected *intraperitoneal* with either 22 mg/kg MAM, (26 mg/ml concentration accounting for liquid density), or vehicle sham (0.9% saline) on gestational day 17. For proteomic and metabonomic experiments, rats were killed at 3 months by cervical dislocation. Brains were dissected on ice, frozen in liquid nitrogen and stored at -80 °C until use. For electrophysiological recordings, samples were prepared as described below.

Tissue fractionation

Frontal cortex and hippocampal tissues from 10 MAM and 10 sham rats were homogenized. For quality control purposes, control rat frontal cortex and hippocampus samples were homogenized, split into 5 aliquots and prepared in parallel with the MAM and sham samples. Two fractions were produced using the ProteoExtract®

Subcellular Proteome Extraction Kit (Calbiochem; Darmstadt, Germany). Both fractions were stored at -80 °C until use. In an independent experiment, a frontal cortex homogenate was split into 12 aliquots, fractionated as above and the resulting samples (fraction 2) were divided randomly into two groups of six for method validation. Each group was spiked with 4 non-homologous proteins (porcine albumin, bovine asialofetuine, bovine casein β and human lactogen) at the indicated concentrations (**Figure 1a**).

Liquid chromatography

Proteins in fraction 1 and 2 (200 µg each) were precipitated using the ProteoExtract® Precipitation Kit (Calbiochem). The resulting pellets were digested using the ProteoExtract® All-in-one Trypsin Digestion Kit (Calbiochem). All further analyses were carried out in triplicate. Separation of the resulting peptides was achieved using a reverse phase C18 column (inner diameter = 75 µm, length = 200 mm, particle size = 1.7µm, Waters Corporation; Milford, MA, USA) on a nano Acquity™ system (Waters Corporation). Buffer A consisted of 0.1% formic acid in water and buffer B was 0.1% formic acid in acetonitrile. The peptides were separated at a flow rate of 0.3 µl/min using the following gradient: 0-90 min, 3% - 30% B; 90-115 min, 30% - 90% B; 115-125 min, 90% B; 125-126 min, 90% - 3% B; 126-150 min, 3% B.

Mass spectrometry

Eluting peptides were ionized at the electrospray interface and analyzed in positive ion mode using a Q-TOF Premier™ mass spectrometer (Waters Corporation), operated in alternate scanning data independent acquisition configuration for label-free peptide quantification and identification (MS^E) (Silva *et al*, 2005). Precursor ion (MS, 0.6 sec) and fragment ion (MS^E, 0.6 sec) spectra were acquired continuously. External reference spectra of [Glu1]-fibrinopeptide B were recorded every 30 seconds for mass correction.

Data processing and protein identification

The data generated were processed and queried against the rat portion of the SwissProt database (release 55.6, 2008-06) using ProteinLynx Global Server v2.3 (Waters Corporation) as described (Geromanos *et al*, 2009; Li *et al*, 2009). Data filtering for peptides was performed using the free statistical software package R (http://cran.r-project.org). The filtering criteria required that peptides were: (i) identified by database searching, (ii) present in at least 2 of the 3 LC-MS_E replicates and (iii) present in at least 80% of the samples of

each treatment group. Quantitative peptide measurements for each replicate were normalized against the total ion volume of all de-convoluted spectra. Replicates were averaged and ratios of protein abundance for each protein calculated based on the sum of peptides. Significance of protein expression differences was determined using Student's t-test with Welch's correction ($p<0.05$). False discovery rate (FDR) was used to control for multiple hypothesis testing ($q<0.5$) (Benjamini and Hochberg, 1995; Storey, 2002).

***In silico* pathway analysis**

The most significant molecular functions, canonical pathways and interactions represented by the integrated lists of significantly altered proteins or metabolites in the MAM-E17 rat model were determined *in silico* using the Ingenuity Pathway Analysis Knowledge Base (IPKB; Ingenuity® Systems; http://www.ingenuity.com) (Calvano *et al*, 2005). The IPKB contains molecular information available in the scientific literature. Lists of the significantly altered proteins or metabolites found in the MAM-E17 rat model were uploaded to the IPKB software (inclusion criterion for proteins: $p<0.05$, $q<0.05$; and metabolites: $p<0.05$).

The functional and pathway analysis identified the biological functions that were most significant to the data set by overlaying the significantly altered molecules (inclusion criterion for proteins: $p<0.05$, $q<0.05$; and metabolites: $p<0.05$) onto predefined maps containing functional and pathway information of the IPKB database. Right-tailed Fisher's exact test was used to calculate a p-value determining the probability that each biological function or pathway assigned to that data set is due to chance alone. Furthermore, network analysis of significantly altered proteins ($p<0.05$, $q<0.05$) was performed. Proteins were mapped to their corresponding objects in the IPKB. Networks were then generated algorithmically based on connectivity derived from molecular interaction information.

Targeted analyte cluster analysis

Complementary to the *in silico* pathway analysis, we applied the targeted analyte cluster (TAC) algorithm as described previously by Cheng et al. (2010) as a means of identifying significantly affected pathways. Significantly changed proteins ($p<0.05$, $q<0.5$) identified by LC-MS^E screening of the MAM-E17 model were subjected to TAC analysis. This method identifies clusters of 2-4 molecules with correlated expression levels

which account for the main variance in the data. This is likely to occur for coordinately-regulated molecules such as those which are components of the same molecular complexes or pathways.

At the statistical level, data points that are not linearly separable in a 2D space can be linearly separated in a higher dimensional (3D) space. TAC applies factor analysis to identify molecules with linear combinations of molecular expression levels, which are the most effective representation of the total variable space of the dataset. Based on the representative molecules identified, the prediction power of the molecular combinations can then be evaluated by testing other datasets using kernel principal component analysis (kPCA). For each prediction, no more than 2-4 molecules are tested to avoid over-fitting in cases of small sample sizes. For example, if a specific combination of proteins A, B and C gives a good separation of MAM and sham rat samples on two dimensional (planar) projections of kPCA, then the protein cluster comprised of A, B and C is likely to be an effective marker for identifying MAM rats. Half of the MAM-E17 and sham rats were selected randomly as a training set. The trained model was applied to predict correct assignment as a MAM or sham rat from the remaining half. The training and prediction procedure was repeated 1000 times. The precision of each protein cluster was calculated finally as the average precision of the 1000 iterations. Precision was defined as the percentage of MAM rats projected correctly.

Immunoblot analysis

Relative differences in abundance of the most significant proteins found using LC-MS^E profiling were tested by immunoblot analysis. Samples of fraction 1 and 2 (10 ug protein) from the same MAM (n=8) and sham (n=8) hippocampal extracts used previously for LC-MS^E analysis, were loaded onto 4-12% NuPAGE Novex Bis-Tris gels (Invitrogen; Paisley, UK) to separate the proteins by electrophoresis. The proteins were then transferred electrophoretically onto polyvinylidene fluoride membranes. Membranes were blocked, incubated with primary and secondary antibodies and then scanned with the Odyssey Infrared Imaging System following the provided protocol (LI-COR Bioscience; Lincoln, NE, USA). The following primary antibodies were used (all from Abcam; Cambridge, UK; dilution indicated in brackets): rabbit anti-AMPA1 (1:200), mouse anti-ARP3 (1:10000), rabbit anti-GAPDH (1:1000), mouse anti-GAPDH (1:1000), rabbit anti-HPCA (1:400), rabbit anti-MARCKS (1:5000), rabbit anti-PMCA1 (1:500) and rabbit anti-SYNJ1 (1:300). In addition, the following secondary antibodies were used (LI-COR Bioscience): donkey anti-mouse IRDye® 800CW and donkey anti-rabbit IRDye® 680

(both 1:15000). Quantification of the infrared signals was performed with the analysis software provided. For normalization of the protein signals, GAPDH was used as a loading control. Only scanned blots with a relative standard deviation of less than 30% for the GAPDH signal were considered. The significance of protein band expression differences were determined using t-test statistics with Welch's correction ($p<0.05$).

To identify the unpredicted band in the AMPA1 immunoblot of fraction 2, a pooled sample of fraction 2 was split into 2 aliquots. One aliquot was treated with λ-protein phosphatase following the protocol provided (New England Biolabs Inc.; Ipswich, MA). Proteins of both aliquots were subjected to immunoblot analysis and probed with phospho-specific rabbit anti-phosphoSerin845 and rabbit anti-phosphoSerin831 AMPA1 antibodies (Abnova; Taipei City, Taiwan; both 1:1000) as described above.

^{1}H-nuclear magnetic resonance (NMR) spectroscopy analysis

Striatum (20 mg), hippocampus (20 mg), frontal cortex (30 mg) and cerebellum (65 mg) of 10 MAM and 10 sham samples were homogenized in 1 ml acetonitrile:deionised water (1:1). The homogenates were combined with an equal volume of 3:1 chloroform:methanol, forming aqueous and lipid phases. The phases were vortexed to homogeneity and centrifuged for 7 minutes at 1200 x g at 5 ^{o}C. The aqueous phase was collected, left overnight at room temperature to remove residual acetonitrile by air drying and then freeze-dried at -70 °C. The samples were reconstituted in 600 µl of deuterium oxide (D_2O). For each sample, a ^{1}H-NMR spectrum was acquired at 600.13 MHz on a Bruker DRX-600 spectrometer (Bruker GmBH) using the first increment of the NOESY pulse sequence (RD, $\pi/2$-$t1$-$\pi/2$-tm-$\pi/2$; TR) as described previously (Lan *et al*, 2009). For each spectrum, 256 transients were acquired to yield 32,000 data points, with a spectral width of 10 kHz at an ambient probe temperature of 25 ^{o}C. The resulting free induction decays were multiplied by an exponential weight function corresponding to a line broadening of 0.3 Hz, prior to Fourier transformation. Complete spectra in the chemical shift range 0.20-10 ppm were phased, baseline-corrected and calibrated according to the reference resonance at 1.33 ppm (lactate doublet), using the Topspin v2.0 software (Bruker GmBH). Spectral variation effects due to pre-saturation of water were removed by zeroing intensity values between 4.5 and 4.9 ppm. To identify metabolites that differentiate MAM from sham animals, partial least squares discriminate analysis (PLS-DA) was performed on full resolution ^{1}H-NMR spectral data using SIMCA-P v12 (Umetrics AB; Umeå, Sweden). To remove confounding variations, orthogonal-projection on latent structures discriminant analyses (OPLS-DA) of full resolution spectra were conducted as described previously (Cloarec *et*

al, 2005). This method is an improvement compared to the traditional supervised algorithm of PLS and enhances the interpretability of spectral variation between classes (Eriksson *et al*, 2004; Lan *et al*, 2009). To confirm the differences identified by multivariate testing, univariate analyses on manually integrated single resonance groups were performed (Student's t-test, $p<0.05$). Pathways and functions associated with significantly altered metabolites were determined using *in silico* pathway analysis as described above.

Electrophysiological recordings

Electrophysiological recordings were made from transverse dorsal hippocampal slices (400 µm) prepared from 3-4 month-old MAM and sham rats. The experimenter was blind to the treatment group. Animals were anaesthetized using isofluorane and killed by cervical dislocation. Brains were removed and placed in ice-cold artificial cerebrospinal fluid (aCSF; 124 mM NaCl, 3 mM KCl, 26 mM $NaHCO_3$, 1.25 mM NaH_2PO_4, 10 mM $MgSO_4$, 10 mM glucose, 1 mM $CaCl_2$) aerated with 95% O_2 and 5% CO_2. Hippocampi were removed, sliced and maintained at 5 ^oC in a 765-1 temperature controlled chamber. The CA3 region was removed and the slices were transferred to aCSF containing 1 mM $MgSO_4$ and 2 mM $CaCl_2$. Slices were incubated at 32 ^oC for 30 minutes to stimulate metabolism and then maintained at room temperature for at least 1 hour before recordings were made.

Extracellular recordings were made in a Slicemate submerged chamber (Scientifica Ltd.; Bedford, UK) maintained at 32 ^oC and continuously perfused at 2 ml per minute with aCSF modified to contain 1 mM $MgSO_4$ and 2 mM $CaCl_2$, and aerated as above. Standard extracellular recording techniques were used to measure the slope of field excitatory post-synaptic potentials (fEPSPs) from stratum radiatum in area CA1, evoked by stimulation of the Schaffer collateral by current injection using a concentric bipolar electrode. Recordings were made with an Axopatch 200B amplifier (Molecular devices Inc.; Silicon Valley, CA, USA), filtered at 2 kHz, and digitized using a Digidata 1322A A/D board at a sampling rate of 10 kHz. In pharmacological experiments using GYKI53784 recordings were filtered at 10 kHz and digitized at 40 kHz, followed by post filtering with a digital gaussian filter to an effective cut off frequency of 1 kHz. Recordings were monitored and analyzed on line and reanalyzed off line using WinLTP (Anderson and Collingridge, 2001). Pharmacological studies were performed to confirm the type of glutamate receptor responsible for synaptic transmission. Baseline responses were set at 5-10 % of the maximal fEPSP obtained at 300 µA stimulation. Following a stable baseline period of at least

20 minutes, 10 µM GYKI53784 (n = 5 and n = 5 for MAM and sham rats, respectively) and 50 µM 2-amino-5-phosphonopentanoic acid (AP5; n = 9 and n = 10 for MAM and sham rats, respectively) were applied in the bath solution for 20 mins. To investigate the efficiency of synaptic transmission, 19 MAM slices and 11 sham slices from 2 batches were stimulated at a range of intensities that resulted in comparable FV amplitudes. Four recordings were made at each stimulation strength at 0.033 Hz and the recordings averaged. fEPSPs were related to the fibre volley (FV) rather than the stimulation strength. This was carried out as the FV is a measure of the action potentials generated in the Schaffer collateral by the stimulating electrode and is therefore the most direct input to synapses in area CA1. Linear regression was performed on the data produced using Prism software v5 (GraphPad). Data is presented as mean ± standard error of mean (SEM). Significant differences between MAM and sham samples were assessed using paired Student's t-tests in the pharmacological experiments and an unpaired Student's t-test in the comparison of the slopes of the input-output relationships between groups ($p<0.05$).

RESULTS

Technical validation of LC-MS^E brain tissue proteomics

The variation introduced by sample preparation and analysis can have a significant impact on the reliability of quantitative molecular profiling experiments. Protein quantification using LC-MS-based approaches has been challenged by physicochemical effects, which can obscure the linear relationship between the signal and abundance of an analyte (King *et al*, 2000). This is especially the case for complex samples such as tissue lysates. Therefore, we assessed the reproducibility and accuracy of the tissue extraction and LC-MS^E procedure in a validation experiment. A homogenized rat cortex sample was divided into 12 aliquots to generate technical replicates. After fractionation the technical replicates were split in two equal groups (A and B) and spiked with non-rat proteins. **Figure 1a** shows the concentrations of the spiked proteins in both groups simulating differential protein abundances between them. All 12 technical replicates were analyzed using LC-MS^E. To assess the reproducibility, the relative standard deviations (RSD) and abundance ratios for 198 identified rat proteins were calculated and plotted (**Figure 1b** and **c**). **Figure 1b** shows that the original protein abundance in the technical replicates deviated by 22% on average, due to sample preparation and analysis. We found in a previous study that approximately 10% of the technical variation was introduced by the LC-MS^E

analysis method (data not shown). This is comparable to or better than other proteomics methods, which show an average variation of 19-30% from the analysis phase alone (Molloy *et al*, 2003; Molloy *et al*, 2005). In addition, the protein abundance ratio distribution in **Figure 1c** illustrates that the relative protein measurements differed by only 4% from the ideal ratio of 1. Comparison of the simulated and measured fold changes of the four spiked non-rat proteins showed that the average deviation of the simulated expression difference was 20% (**Figure 1a**). The values for the individual proteins vary possibly due to different physicochemical properties of the proteins resulting in different ionization efficiencies (King *et al*, 2000). We also obtained a similar result using 20 aliquots of serum samples, which required fewer sample preparation steps (Levin *et al*, 2007). Consequently, the data showed that the integration of quality controls for LC-MS^E analysis of brain tissue was necessary in order to assess the precision of the quantitative measurement for each protein. This guarantees a more accurate interpretation of the data.

LC-MS^E analysis of MAM rat frontal cortex and hippocampus

Analysis of fraction 1 and 2 of frontal cortex from MAM rats by LC-MS^E resulted in identification of 743 proteins (data not shown). None of these proteins showed significant differences in expression between the MAM and sham rats ($q>0.99$). LC-MS^E analysis of hippocampus from MAM rats resulted in identification of 673 proteins (data not shown) and 38 of these showed statistically significant differences in expression ($p<0.05$, $q<0.5$; **Table 1**). After controlling for multiple hypotheses testing, 6 proteins (AMPA1, ARP3, MARCKS, HPCA, PMCA1 and SYNJ1) showed FDR q-values of less than 0.05. The protein expression differences ranged between 6-25% and could be measured with an average RSD of 7%. This low variability of the protein abundance (**Figure 1a**) provides confidence in the detection of subtle expression differences such as seen here and thereby provides greater reliability of the candidate proteins.

Validation of LC-MS^E hippocampal candidate proteins by immunoblot analysis

Six candidate proteins, showing the greatest significance after controlling for FDR ($q<0.05$), were selected for validation. Due to a lack of commercially available immunoassays for these proteins, we tested the candidate proteins using immunoblot analysis, which is considered to be a semi-quantitative method (Mann, 2008). We used an infrared fluorescence detection system improving quantification (Schutz-Geschwender *et al*, 2004) and were able to confirm the altered expression of PMCA1, HPCA and MARCKS ($p<0.05$; MAM, n=8; sham,

n=8) despite expression differences of only 7-21% (**Figure 2a** and **b**). We could not confirm expression differences for ARP3 and SYNJ1, most likely since these showed only 7-11% changes based on the LC-MS^E analysis. Interestingly, AMPA1 immunoblots of fraction 2 identified two bands. Further immunoblot experiments (**Figure 2c**) showed that the predicted 95 kDa band corresponds to the non-phosphorylated form of the protein while the upper band represents a phosphorylated form (at Serine-845/Serine-838 (Mammen *et al*, 1997)). Neither of these bands was expressed at significantly different levels. However, the ratio between the upper and lower band did show a significant difference between MAM and sham rats (p=0.014), suggesting a potential reduced level of phosphorylated AMPA1 receptor in MAM rats. Comparison of the measurements of each protein by LC-MS^E and immunoblot analysis showed significant correlations for PMCA1, HPCA and the upper AMPA1 band (**Figure 2b**).

***In silico* pathway analysis of differentially expressed hippocampal proteins**

We used the IPKB software, for *in silico* characterization of the 38 differentially expressed hippocampal proteins ($p<0.05$, $q<0.5$; **Table 1**). The SwissProt accession number of each protein was uploaded into the software and these were mapped onto the predefined IPKB global network. Global pathway analysis of all 38 differential expressed hippocampal proteins ($p<0.05$, $q<0.5$; **Table 1**) showed that the most significant function associated with the altered proteins were related to cell-to-cell signaling and neuronal function (n=23 proteins associated with function, **Figure 3a**). At the level of canonical pathways, the three most significant associations with the 38 differentially expressed proteins ($p<0.05$, $q<0.5$; **Table 1**) were calcium signaling (n=8 proteins, Fisher's exact test p-value = $9.34x10^{-9}$), synaptic long term potentiation (n=6 proteins, Fisher's exact test p-value = $2.65x10^{-7}$) and glutamate receptor signaling (n=4 proteins, Fisher's exact test p-value = $1.19x10^{-5}$) (**Figure 3b**). The proteins assigned to these pathways are subsets of the functional network previously identified by functional analysis (**Figure 3a and b**).

Furthermore, the IPKB software detected significant molecular interaction of 22 of the 38 differentially expressed hippocampal proteins ($p<0.05$, $q<0.5$; **Table 1**) using network analysis (Fisher's exact test p-value =$1x10^{-53}$, **Figure 3c)**. Proteins of the network are involved in nervous system development and function. Ten of the network proteins (AMPH, ATP1A1, CAMK2A, CAMK2D, AMPA1, AMPA2, NCAM1, PPP3CA, SYNJ1, TUBA8) have been associated previously with psychological disorders such as bipolar affective disorder

(n=8 proteins), schizophrenia (n= 6 proteins) and major depressive disorder (n=4 proteins) (see IPKB database for further details).

Cluster analysis of differentially expressed proteins in the MAM rat hippocampus

We next attempted to identify clusters of co-behaving proteins among the 38 significantly altered proteins ($p<0.05$, $q<0.5$; **Table 1**) which contribute most to the differences observed in the hippocampus between MAM and sham rats. Co-behavior was examined by targeted analyte cluster (TAC) analysis (Cheng *et al*, 2010) as described in the methods. This led to identification of four clusters of proteins in fraction 2 which gave 100% precision for correct classification of MAM and sham hippocampi after iterative testing (precision was defined as the proportion of MAM samples predicted correctly). The proteins forming the four clusters (# 1 (AMPA2 + PPP3CA + SYNJ1), # 2 (AMPA1 + AMPA2 + PPP3CA), #3 (AMPA1 + PMCA1 + PPP3CA), # 4 (AMPA1 + AMPA2 + HPCA1) have been previously mapped to cell-cell signaling and neuronal function by functional analysis using IPKB (**Figure 3a**). Interestingly, the clusters describe proteins involved in calcium and glutamate receptor signaling, as previously identified using IPKB (**Figure 3b**). This highlighted the importance of these pathways for the hippocampal pathology in the MAM-E17 model as each of these clusters predicted MAM-E17 and sham rats correctly based only on the expression patterns of the 3 cluster proteins.

^{1}H-NMR spectroscopic analysis

To study the effect of MAM-treatment on brain metabolites, ^{1}H-NMR spectra were acquired for frontal cortex, hippocampus, striatum and cerebellum. The PLS-DA analysis indicated differences in the metabolic profiles of the hippocampus (Q^2(cum)=0.62, **Figure 4a**). No statistically robust PLS-DA model could be constructed for the other brain regions. A representative and annotated spectrum of a sham animal is presented in **Figure 4b**. OPLS-DA analysis was conducted to identify the metabolites responsible for the differences between MAM and sham hippocampi. The coefficients plot of the model indicated disparities in the spectral regions of *scyllo*-inositol, phosphocholine (PC), glutamate, N-acetyl aspartyl glutamate (NAAG), overlapping spectral regions of N-acetyl aspartate (NAA)/aspartate and glutamate/glutamine (**Figure 4c**). Manual integration of spectra was conducted to verify and quantify the differences found by multivariate analysis (**Figure 4d**). Only spectral regions showing resonances of single metabolites were considered. The metabolic profile changes seen in the OPLS-DA model were confirmed with exception of the aspartate/NAA signal. These analytes showed signal

changes only in an overlapping region of the spectrum. Confirmation of the difference in NAAG levels identified by multivariate statistics was not possible as other metabolites interfere with the signal of all NAAG resonance groups. However, the integration of the alanine and the glycine region showed significantly lower levels in MAM compared to sham rats.

Pathway analysis of the metabolites responsible for the differences between MAM and sham showed that glutamate receptor signaling was the most significant canonical pathway affected ($p=0.000002$). Furthermore, enzymes and transporters of the glutamate-glutamine cycle, which were found to be changed in the LC-MS^E analysis, are known to facilitate inter-conversion of glutamate and glutamine in astrocytes and neurons. In addition, many significantly changed metabolites seem to be connected in an interaction network. Neuropeptide and NMDA receptor antagonist NAAG is cleaved by neuropeptidase glutamate carboxypeptidase II (GCPII) to NAA and glutamate (Slusher *et al*, 1990) and NMDA agonist glycine, alanine and glutamine can be reversibly converted by transaminase reactions.

Electrophysiological analysis of MAM rat hippocampal slices

The proteomic and metabonomic results indicated changes of molecules involved in neuronal transmission in the hippocampus of MAM-E17 rats. In particular, proteins and metabolites of the glutamate receptor signaling pathway, as identified by *in silico* pathway and TAC analysis, seem to be effected in both studies. To test this, we investigated glutamatergic synaptic transmission using electrophysiological recordings in the CA1 area of the hippocampus. Previous studies have shown that synaptic transmission in this area is mediated by AMPA receptors (Andreasen *et al*, 1989; Davies and Collingridge, 1989). To investigate if AMPA receptor changes alter excitatory synaptic function in MAM rats, synaptic transmission was investigated. In order to confirm that synaptic transmission is mediated by AMPA receptors in our preparation, the AMPA receptor antagonist GYKI53784 (10 μM) was applied and found to block synaptic transmission in both sham and MAM slices. Average fEPSPs in sham slices were 0.04 ± 0.01 V/s and 0.30 ± 0.04 V/s in the presence and absence of GYKI53784, respectively (**Figure 5a**, $p<0.05$). Average fEPSPs in MAM slices were 0.02 ± 0.01 V/s and 0.21 ± 0.02 V/s in the presence and absence of GYKI53784, respectively (**Figure 5b**, $p<0.05$). Conversely, the NMDA receptor antagonist 2-amino-5-phosphonopentanoic acid (AP5, 50 μM) did not affect synaptic transmission in either sham or MAM slices. Average fEPSPs in sham slices were 0.47 ± 0.03 V/s and 0.49 ± 0.03 V/s in the

presence and absence of AP5, respectively (**Figure 5c**, p>0.05). Average fEPSPs in MAM slices were 0.36 ± 0.04 and 0.35 ± 0.03 V/s in the presence and absence of AP5, respectively (**Figure 5d**, p>0.05). FVs and fEPSPs were then recorded at a range of stimulation strengths. Comparative analysis showed that for any given FV, the fEPSP generated was significantly reduced in slices from MAM rats compared to those from sham rats (**Figure 5e and f**). Quantification of the FV versus fEPSP relationship by linear regression analysis of the MAM data set gave a slope of 0.68 ± 0.16 ms^{-1}, compared to 1.24 ± 0.15 ms^{-1} in sham slices (p<0.05) **(Figure 5g)**. This suggested a deficit in AMPA receptor-mediated synaptic transmission.

DISCUSSION

The present study describes the first molecular characterization, combined with a functional validation, of the MAM-E17 rat model for schizophrenia. The combined use of two molecular profiling platforms demonstrated that MAM administration on E17 had a significant impact on protein and metabolite levels in the hippocampus. The frontal cortex did not show any significant molecular effects of prenatal MAM exposure, even though neuroanatomical changes have been reported for this brain region (Moore *et al*, 2006). However, previous studies have shown that the frontal cortex has milder morphological effects in response to MAM-treatment compared to those reported in the hippocampus (Flagstad *et al*, 2004; Lodge *et al*, 2009a; Matricon *et al*, 2010; Moore *et al*, 2006; Penschuck *et al*, 2006). Therefore, it is possible that such subtle changes might not lead to detectable molecular correlates in whole tissue lysates using the current methodologies.

Many of the differentially expressed proteins and metabolites in the hippocampus appeared to be components of an *in silico*-determined interaction network suggesting significant effects of embryonic MAM-treatment on neuronal signal transduction. MAM-treatment may affect neurotransmission by altering the levels of specific neurotransmitters, glutamate receptor agonists/antagonists, glutamate-glutamine cycle proteins or synaptic vesicle controlling proteins. The data showed that MAM-treatment may alter synaptic neurotransmission by affecting the extent or innervation and/or post-synaptic signal transduction mechanisms through alterations in AMPA receptor subunit expression or phosphorylation, clathrin-mediated receptor internalization and calcium signaling as identified by *in silico* pathway analysis and supported by TAC analysis. As a variety of molecules involved in neurotransmission were found to be altered, this may indicate that

multiples of these possibilities might play a synergistic role. The potential functional consequences of the molecular changes identified in the hippocampus were analyzed by in vitro electrophysiology in hippocampal slices. The fEPSPs recordings in slices from MAM-treated rats showed a reduction in glutamatergic synaptic transmission. In particular, they are compatible with less expression of phosphorylated AMPA1 subunits, as preliminary biochemical data showed. Phosphorylation of AMPA1 is known to have dramatic effects on both AMPA receptor trafficking and gating. Not only highly relevant synaptic plasticity events such as long-term potentiation, long-term depression and depotentiation depend on AMPA1 phosphorylation, but in AMPA1 "phosphorylation-deficient" transgenic mice, specific cognitive deficits relevant to schizophrenia were also found (Lee *et al*, 2003). Finally, it is worth mentioning that while the recordings suggested a reduction in AMPA receptor-mediated synaptic transmission of potential post-synaptic origin, we cannot exclude at this stage that some of the functional deficits and molecular alterations could also be caused by further changes in innervation, total number of synapses formed, or functional alteration in the interplay between neurons and glia cells at synapses in the hippocampi of MAM rats (Matricon *et al*, 2010). Further studies to identify and confirm the molecular basis of the synaptic deficits, investigating more complex aspects of synaptic plasticity and combining morphometric and immunohistological methods, are warranted given the potential relevance of this model for schizophrenia research and drug development.

The importance of the hippocampus in the pathology of schizophrenia has been the focus of several studies. Most of the evidence derives from *post mortem* or neuropsychological studies and many of the findings are consistent with those found in the MAM-E17 model. The most reproducible effect in patients with schizophrenia appeared to be a reduction of hippocampal size (Bogerts *et al*, 1990; Lawrie *et al*, 1999; Shenton *et al*, 2001), which is evident in MAM rats (Featherstone *et al*, 2007; Moore *et al*, 2006). Similarly, *post mortem* studies of schizophrenia patients show disarray of pyramidal cells and a decrease in parvalbumin-expressing interneurons in the hippocampus (Kovelman and Scheibel, 1984; Zhang and Reynolds, 2002), as reported for MAM rats (Flagstad *et al*, 2004; Moore *et al*, 2006; Penschuck *et al*, 2006). The assignment of neuropsychological deficits in mental illnesses to specific brain structures has been a controversial subject. However, there have been suggestions that the hippocampus is involved in sensorimotor gating and latent inhibition (Gothelf *et al*, 2000; Gray *et al*, 1995; Swerdlow *et al*, 2001), both of which are deficient in schizophrenia patients (Braff, 1993; Braff *et al*, 2001; Braff *et al*, 1992; Gray, 1998) and adult MAM rats (Flagstad *et al*, 2005; Le Pen *et al*, 2006; Lodge *et al*, 2009a; Moore *et al*, 2006).

Functional and *post mortem* studies of schizophrenia patients have shown a reduced neuronal activity and altered synaptic markers in the hippocampus, implying disrupted neuronal function (Gao *et al*, 2000; Medoff *et al*, 2001; Nesvaderani *et al*, 2009; Tamminga *et al*, 1992; Tsai *et al*, 1995). The most consistent findings point towards a glutamatergic synaptic pathology in schizophrenia. Various studies have shown that glutamate levels, glutamate receptors, glutamate transport and neurotransmitter vesicle molecules are altered in the hippocampus of patients with schizophrenia (Eastwood *et al*, 1995b; Gao *et al*, 2000; Harrison *et al*, 2003; Hemby *et al*, 2002; Knable *et al*, 2004; Tsai *et al*, 1995; Webster *et al*, 2001). Similar effects have been demonstrated in the present study for MAM rats at both the molecular and functional levels, reflecting some aspects of the glutamatergic hypothesis of schizophrenia (Kim *et al*, 1980). Not all of the molecular changes observed in hippocampi of schizophrenia patients have been detected in the MAM rats (Eastwood *et al*, 1995a; Eastwood and Harrison, 1998; Fatemi *et al*, 2000), although the same pathways and cellular functions were found to be affected as identified by *in silico* pathway analysis and supported by TAC analysis. Such molecular changes may result from a decreased number of total synapses, defective synaptic coupling or a change in the neuropil formation as suggested by Matricon and colleagues for the MAM-E17 model (Matricon *et al*, 2010) and demonstrated in cases of human schizophrenia subjects (Garey, 2010).

Future directions and conclusion

The combined use of a proteomics approach with complementary molecular and functional studies has resulted in identification and validation of a significant effect on glutamate neurotransmission in the offspring of MAM-treated rats. Nevertheless, the origin of these changes in the hippocampus is unclear. LC-MS^E profiling of whole hippocampal tissue as used here does not take into account cell morphological and subfield-specific expression differences as seen in schizophrenia studies (Benes *et al*, 1991; Eastwood *et al*, 1995b; Gao *et al*, 2000; Garey, 2010; Knable *et al*, 2004). Therefore, we suggest that future studies should investigate subcellular and subregional expression and phophorylation patterns of synaptic markers and glutamatergic indices, as identified in this study, in combination with synaptic structure and density measurements in hippocampal subfields of the MAM-E17 rat model. In addition, further investigation of the functional markers NAA (Simmons *et al*, 1991), aspartate and related molecules is of interest as these have also been found to be reduced in hippocampi of schizophrenia patients (Bertolino *et al*, 1996; Deicken *et al*, 1998; Maier *et al*, 1995; Tsai *et al*, 1995). A reduction in NAA might result from reduced GCPII activity as seen in schizophrenia (Tsai *et*

al, 1995). This enzyme is known to cleave NAAG to produce NAA and glutamate, which were both changed significantly in the present study.

It is now accepted that animal models *per se* can recapitulate only certain aspects of neuropsychiatric disease. The present studies showed that MAM-treatment of rats may lead to an altered glutamatergic neurotransmission in the hippocampus, although the exact cause of this deficit remains to be elucidated. Nevertheless, this study provides the first molecular evidence, combined with functional validation, that the MAM-E17 rat model reproduces hippocampal deficits relevant to the pathology of schizophrenia. Further investigation of these deficits using this model may lead to further insights into the hypo-glutamatergic hypothesis of schizophrenia and demonstrate its potential utility for drug discovery and development.

DISCLOSURE

E. Hradetzky was supported by a BBSRC CASE award jointly with Eli Lilly and Co Ltd. TM. Sanderson, JL. Sherwood, SM. Fitzjohn, V. Lakics, N. Malik, MJ. O'Neill, E. Sher and MD. Tricklebank are full-time employees of Eli Lilly and Co Ltd and receive no other financial remuneration. GL. Collingridge is supported by the Medical Research Council. PC. Guest and H. Rahmoune are consultants for Psynova Neurotech. The other authors declare that no financial support or compensation has been received from any individual or corporate entity for research or professional service and there are no personal financial holdings that could be perceived as constituting a potential conflict of interest. The research was supported by the IMI NEWMEDS European Framework Programme (FP7) and Stanley Medical Research Institute (SMRI).

ACKNOWLEDGEMENTS

We thank Dan Ma, Sandra Pietsch and Christin Oheim for help with the dissection of the rat brains and immunoblots, Yishai Levin and Emanuel Schwarz for helpful discussions.

REFERENCES

*Anderson WW, Collingridge GL (2001). The LTP Program: a data acquisition program for on-line analysis of long-term potentiation and other synaptic events. J Neurosci Methods **108**(1): 71-83.*

*Andreasen M, Lambert JD, Jensen MS (1989). Effects of new non-N-methyl-D-aspartate antagonists on synaptic transmission in the in vitro rat hippocampus. J Physiol **414**: 317-336.*

*Bayer SA, Altman J, Russo RJ, Zhang X (1993). Timetables of neurogenesis in the human brain based on experimentally determined patterns in the rat. Neurotoxicology **14**(1): 83-144.*

*Benes FM, Sorensen I, Bird ED (1991). Reduced neuronal size in posterior hippocampus of schizophrenic patients. Schizophr Bull **17**(4): 597-608.*

Benjamini J, Hochberg Y (1995). Controlling the false discovery rate: a practical and powerful approach to multiple testing. J Roy Statist Soc.

*Bertolino A, Nawroz S, Mattay VS, Barnett AS, Duyn JH, Moonen CT, et al (1996). Regionally specific pattern of neurochemical pathology in schizophrenia as assessed by multislice proton magnetic resonance spectroscopic imaging. Am J Psychiatry **153**(12): 1554-1563.*

*Bogerts B, Ashtari M, Degreef G, Alvir JM, Bilder RM, Lieberman JA (1990). Reduced temporal limbic structure volumes on magnetic resonance images in first episode schizophrenia. Psychiatry Res **35**(1): 1-13.*

*Braff DL (1993). Information processing and attention dysfunctions in schizophrenia. Schizophr Bull **19**(2): 233-259.*

*Braff DL, Geyer MA, Light GA, Sprock J, Perry W, Cadenhead KS, et al (2001). Impact of prepulse characteristics on the detection of sensorimotor gating deficits in schizophrenia. Schizophr Res **49**(1-2): 171-178.*

*Braff DL, Grillon C, Geyer MA (1992). Gating and habituation of the startle reflex in schizophrenic patients. Arch Gen Psychiatry **49**(3): 206-215.*

*Calvano SE, Xiao W, Richards DR, Felciano RM, Baker HV, Cho RJ, et al (2005). A network-based analysis of systemic inflammation in humans. Nature **437**(7061): 1032-1037.*

*Cattabeni F, Di Luca M (1997). Developmental models of brain dysfunctions induced by targeted cellular ablations with methylazoxymethanol. Physiol Rev **77**(1): 199-215.*

*Cattaneo E, Reinach B, Caputi A, Cattabeni F, Di Luca M (1995). Selective in vitro blockade of neuroepithelial cells proliferation by methylazoxymethanol, a molecule capable of inducing long lasting functional impairments. J Neurosci Res **41**(5): 640-647.*

*Cheng TM, Lu YE, Guest PC, Rahmoune H, Harris LW, Wang L, et al (2010). Identification of targeted analyte clusters for studies of schizophrenia. Mol Cell Proteomics **9**(3): 510-522.*

*Cloarec O, Dumas ME, Trygg J, Craig A, Barton RH, Lindon JC, et al (2005). Evaluation of the orthogonal projection on latent structure model limitations caused by chemical shift variability and improved visualization of biomarker changes in 1H NMR spectroscopic metabonomic studies. Anal Chem **77**(2): 517-526.*

*Davies SN, Collingridge GL (1989). Role of excitatory amino acid receptors in synaptic transmission in area CA1 of rat hippocampus. Proc R Soc Lond B Biol Sci **236**(1285): 373-384.*

*Deicken RF, Zhou L, Schuff N, Fein G, Weiner MW (1998). Hippocampal neuronal dysfunction in schizophrenia as measured by proton magnetic resonance spectroscopy. Biol Psychiatry **43**(7): 483-488.*

*Eastwood SL, Burnet PW, Harrison PJ (1995a). Altered synaptophysin expression as a marker of synaptic pathology in schizophrenia. Neuroscience **66**(2): 309-319.*

*Eastwood SL, Harrison PJ (1998). Hippocampal and cortical growth-associated protein-43 messenger RNA in schizophrenia. Neuroscience **86**(2): 437-448.*

*Eastwood SL, McDonald B, Burnet PW, Beckwith JP, Kerwin RW, Harrison PJ (1995b). Decreased expression of mRNAs encoding non-NMDA glutamate receptors GluR1 and GluR2 in medial temporal lobe neurons in schizophrenia. Brain Res Mol Brain Res **29**(2): 211-223.*

*Eriksson L, Antti H, Gottfries J, Holmes E, Johansson E, Lindgren F, et al (2004). Using chemometrics for navigating in the large data sets of genomics, proteomics, and metabonomics (gpm). Anal Bioanal Chem **380**(3): 419-429.*

*Fatemi SH, Earle JA, McMenomy T (2000). Reduction in Reelin immunoreactivity in hippocampus of subjects with schizophrenia, bipolar disorder and major depression. Mol Psychiatry **5**(6): 654-663, 571.*

*Featherstone RE, Rizos Z, Nobrega JN, Kapur S, Fletcher PJ (2007). Gestational methylazoxymethanol acetate treatment impairs select cognitive functions: parallels to schizophrenia. Neuropsychopharmacology **32**(2): 483-492.*

*Flagstad P, Glenthoj BY, Didriksen M (2005). Cognitive deficits caused by late gestational disruption of neurogenesis in rats: a preclinical model of schizophrenia. Neuropsychopharmacology **30**(2): 250-260.*

*Flagstad P, Mork A, Glenthoj BY, van Beek J, Michael-Titus AT, Didriksen M (2004). Disruption of neurogenesis on gestational day 17 in the rat causes behavioral changes relevant to positive and negative schizophrenia symptoms and alters amphetamine-induced dopamine release in nucleus accumbens. Neuropsychopharmacology **29**(11): 2052-2064.*

*Gao XM, Sakai K, Roberts RC, Conley RR, Dean B, Tamminga CA (2000). Ionotropic glutamate receptors and expression of N-methyl-D-aspartate receptor subunits in subregions of human hippocampus: effects of schizophrenia. Am J Psychiatry **157**(7): 1141-1149.*

*Garey L (2010). When cortical development goes wrong: schizophrenia as a neurodevelopmental disease of microcircuits. J Anat **217**(4): 324-333.*

*Geromanos SJ, Vissers JP, Silva JC, Dorschel CA, Li GZ, Gorenstein MV, et al (2009). The detection, correlation, and comparison of peptide precursor and product ions from data independent LC-MS with data dependant LC-MS/MS. Proteomics **9**(6): 1683-1695.*

*Gothelf D, Soreni N, Nachman RP, Tyano S, Hiss Y, Reiner O, et al (2000). Evidence for the involvement of the hippocampus in the pathophysiology of schizophrenia. Eur Neuropsychopharmacol **10**(5): 389-395.*

*Gray JA (1998). Integrating schizophrenia. Schizophr Bull **24**(2): 249-266.*

*Gray JA, Joseph MH, Hemsley DR, Young AM, Warburton EC, Boulenguez P, et al (1995). The role of mesolimbic dopaminergic and retrohippocampal afferents to the nucleus accumbens in latent inhibition: implications for schizophrenia. Behav Brain Res **71**(1-2): 19-31.*

*Hansen CF, Torgalsboen AK, Melle I, Bell MD (2009). Passive/apathetic social withdrawal and active social avoidance in schizophrenia: difference in underlying psychological processes. J Nerv Ment Dis **197**(4): 274-277.*

*Harrison PJ (1999). The neuropathology of schizophrenia. A critical review of the data and their interpretation. Brain **122 (Pt 4)**: 593-624.*

*Harrison PJ, Law AJ, Eastwood SL (2003). Glutamate receptors and transporters in the hippocampus in schizophrenia. Ann N Y Acad Sci **1003**: 94-101.*

*Hemby SE, Ginsberg SD, Brunk B, Arnold SE, Trojanowski JQ, Eberwine JH (2002). Gene expression profile for schizophrenia: discrete neuron transcription patterns in the entorhinal cortex. Arch Gen Psychiatry **59**(7): 631-640.*

*Kim JS, Kornhuber HH, Schmid-Burgk W, Holzmuller B (1980). Low cerebrospinal fluid glutamate in schizophrenic patients and a new hypothesis on schizophrenia. Neurosci Lett **20**(3): 379-382.*

*King R, Bonfiglio R, Fernandez-Metzler C, Miller-Stein C, Olah T (2000). Mechanistic investigation of ionization suppression in electrospray ionization. J Am Soc Mass Spectrom **11**(11): 942-950.*

*Knable MB, Barci BM, Webster MJ, Meador-Woodruff J, Torrey EF (2004). Molecular abnormalities of the hippocampus in severe psychiatric illness: postmortem findings from the Stanley Neuropathology Consortium. Mol Psychiatry **9**(6): 609-620, 544.*

*Kovelman JA, Scheibel AB (1984). A neurohistological correlate of schizophrenia. Biol Psychiatry **19**(12): 1601-1621.*

*Lan MJ, McLoughlin GA, Griffin JL, Tsang TM, Huang JT, Yuan P, et al (2009). Metabonomic analysis identifies molecular changes associated with the pathophysiology and drug treatment of bipolar disorder. Mol Psychiatry **14**(3): 269-279.*

*Laruelle M, Abi-Dargham A, van Dyck CH, Gil R, D'Souza CD, Erdos J, et al (1996). Single photon emission computerized tomography imaging of amphetamine-induced dopamine release in drug-free schizophrenic subjects. Proc Natl Acad Sci U S A **93**(17): 9235-9240.*

*Lawrie SM, Whalley H, Kestelman JN, Abukmeil SS, Byrne M, Hodges A, et al (1999). Magnetic resonance imaging of brain in people at high risk of developing schizophrenia. Lancet **353**(9146): 30-33.*

*Le Pen G, Gourevitch R, Hazane F, Hoareau C, Jay TM, Krebs MO (2006). Peri-pubertal maturation after developmental disturbance: a model for psychosis onset in the rat. Neuroscience **143**(2): 395-405.*

Lee HK, Takamiya K, Han JS, Man H, Kim CH, Rumbaugh G, et al (2003). Phosphorylation of the AMPA receptor GluR1 subunit is required for synaptic plasticity and retention of spatial memory. Cell 112(5): 631-643.

*Levin Y, Schwarz E, Wang L, Leweke FM, Bahn S (2007). Label-free LC-MS/MS quantitative proteomics for large-scale biomarker discovery in complex samples. J Sep Sci **30**(14): 2198-2203.*

*Li GZ, Vissers JP, Silva JC, Golick D, Gorenstein MV, Geromanos SJ (2009). Database searching and accounting of multiplexed precursor and product ion spectra from the data independent analysis of simple and complex peptide mixtures. Proteomics **9**(6): 1696-1719.*

*Lodge DJ, Behrens MM, Grace AA (2009a). A loss of parvalbumin-containing interneurons is associated with diminished oscillatory activity in an animal model of schizophrenia. J Neurosci **29**(8): 2344-2354.*

*Lodge DJ, Grace AA (2009b). Gestational methylazoxymethanol acetate administration: a developmental disruption model of schizophrenia. Behav Brain Res **204**(2): 306-312.*

*Lubow RE, Gewirtz JC (1995). Latent inhibition in humans: data, theory, and implications for schizophrenia. Psychol Bull **117**(1): 87-103.*

*Maier M, Ron MA, Barker GJ, Tofts PS (1995). Proton magnetic resonance spectroscopy: an in vivo method of estimating hippocampal neuronal depletion in schizophrenia. Psychol Med **25**(6): 1201-1209.*

*Mammen AL, Kameyama K, Roche KW, Huganir RL (1997). Phosphorylation of the alpha-amino-3-hydroxy-5-methylisoxazole4-propionic acid receptor GluR1 subunit by calcium/calmodulin-dependent kinase II. J Biol Chem **272**(51): 32528-32533.*

*Mann M (2008). Can proteomics retire the western blot? J Proteome Res **7**(8): 3065.*

*Matricon J, Bellon A, Frieling H, Kebir O, Le Pen G, Beuvon F, et al (2010). Neuropathological and Reelin deficiencies in the hippocampal formation of rats exposed to MAM; differences and similarities with schizophrenia. PLoS One **5**(4): e10291.*

*Medoff DR, Holcomb HH, Lahti AC, Tamminga CA (2001). Probing the human hippocampus using rCBF: contrasts in schizophrenia. Hippocampus **11**(5): 543-550.*

*Meyn RE, Murray D (1984). Cell cycle effects of alkylating agents. Pharmacol Ther **24**(2): 147-163.*

*Molloy MP, Brzezinski EE, Hang J, McDowell MT, VanBogelen RA (2003). Overcoming technical variation and biological variation in quantitative proteomics. Proteomics **3**(10): 1912-1919.*

*Molloy MP, Donohoe S, Brzezinski EE, Kilby GW, Stevenson TI, Baker JD, et al (2005). Large-scale evaluation of quantitative reproducibility and proteome coverage using acid cleavable isotope coded affinity tag mass spectrometry for proteomic profiling. Proteomics **5**(5): 1204-1208.*

*Moore H, Jentsch JD, Ghajarnia M, Geyer MA, Grace AA (2006). A neurobehavioral systems analysis of adult rats exposed to methylazoxymethanol acetate on E17: implications for the neuropathology of schizophrenia. Biol Psychiatry **60**(3): 253-264.*

*Nesvaderani M, Matsumoto I, Sivagnanasundaram S (2009). Anterior hippocampus in schizophrenia pathogenesis: molecular evidence from a proteome study. Aust N Z J Psychiatry **43**(4): 310-322.*

*Penschuck S, Flagstad P, Didriksen M, Leist M, Michael-Titus AT (2006). Decrease in parvalbumin-expressing neurons in the hippocampus and increased phencyclidine-induced locomotor activity in the rat methylazoxymethanol (MAM) model of schizophrenia. Eur J Neurosci **23**(1): 279-284.*

*Schutz-Geschwender A ZY, Holt T, McDermitt D, Olive DM. (2004). Quantitative, two-color Western blot detection with infrared fluorescence. LI-COR Biosciences **URL:*** http://www.licor.com/bio/PDF/IRquant.pdf.

*Shenton ME, Dickey CC, Frumin M, McCarley RW (2001). A review of MRI findings in schizophrenia. Schizophr Res **49**(1-2): 1-52.*

*Silva JC, Denny R, Dorschel CA, Gorenstein M, Kass IJ, Li GZ, et al (2005). Quantitative proteomic analysis by accurate mass retention time pairs. Anal Chem **77**(7): 2187-2200.*

*Simmons ML, Frondoza CG, Coyle JT (1991). Immunocytochemical localization of N-acetyl-aspartate with monoclonal antibodies. Neuroscience **45**(1): 37-45.*

*Slusher BS, Robinson MB, Tsai G, Simmons ML, Richards SS, Coyle JT (1990). Rat brain N-acetylated alpha-linked acidic dipeptidase activity. Purification and immunologic characterization. J Biol Chem **265**(34): 21297-21301.*

*Storey JD (2002). A direct approach to false discovery rates. J R Statist Soc B **64**: 479-498.*

*Swerdlow NR, Geyer MA, Braff DL (2001). Neural circuit regulation of prepulse inhibition of startle in the rat: current knowledge and future challenges. Psychopharmacology (Berl) **156**(2-3): 194-215.*

*Tamminga CA, Thaker GK, Buchanan R, Kirkpatrick B, Alphs LD, Chase TN, et al (1992). Limbic system abnormalities identified in schizophrenia using positron emission tomography with fluorodeoxyglucose and neocortical alterations with deficit syndrome. Arch Gen Psychiatry **49**(7): 522-530.*

*Tsai G, Passani LA, Slusher BS, Carter R, Baer L, Kleinman JE, et al (1995). Abnormal excitatory neurotransmitter metabolism in schizophrenic brains. Arch Gen Psychiatry **52**(10): 829-836.*

*Webster MJ, Shannon Weickert C, Herman MM, Hyde TM, Kleinman JE (2001). Synaptophysin and GAP-43 mRNA levels in the hippocampus of subjects with schizophrenia. Schizophr Res **49**(1-2): 89-98.*

*Zhang ZJ, Reynolds GP (2002). A selective decrease in the relative density of parvalbumin-immunoreactive neurons in the hippocampus in schizophrenia. Schizophr Res **55**(1-2): 1-10.*

TITLES AND LEGENDS TO FIGURES

Figure 1. Technical validation of LC-MS^E proteomics using 12 spiked replicates of rat brain lysates. **a)** Accuracy was assessed by measurement of 4 spiked non-rat proteins simulating different protein abundance ratios in the technical replicates. Reproducibility was assessed using density plots of **b)** the RSD of the protein abundance measurements of 189 rat proteins in each technical replicate and **c)** the relative protein abundance (ideal value = 1).

Figure 2. Immunoblot analysis of differentially expressed hippocampal candidate proteins identified by LC-MS^E. **a)** Western blot images of candidate proteins identified in fraction 1 and 2. MAM and sham samples were loaded alternately to reduce any potential artifactual effects of differential electrotransfer. **b)** Expression ratios and p-values are listed for each fraction. Correlation values are given for the LC-MS^E and immunoblot signals. **c)** Immunoblot characterization of the two AMPA1 receptor bands in rat hippocampal tissue of fraction 2. Anti-AMPA1 receptor immunoblot analysis of MAM and sham hippocampus shows the predicted 95kDa band and an additional band at ~110 kDa (indicated by ←). Phosphatase treated (PP treated) and untreated samples were tested by Western blot analysis with phospo-specific AMPA1 antibodies, demonstrating that the 110 kDa band is reduced in intensity after dephosphorylation. These results suggested that the ~110 kDa band is a phosphorylated form of the AMPA1 receptor. Lanes 1,4,7 and 10 show the position of a 100kDa protein marker.

Figure 3. *In silico* functional, pathway and network analysis of the 38 differentially expressed candidate proteins in the hippocampus of MAM rats (p<0.05, q<0.5; Table 1): The differentially expressed proteins were overlaid onto predefined functional networks and pathways of the IPKB database. Significance of the association with a function and pathway, or protein interaction was calculated using Fisher's exact test. **a)** The table lists the proteins sharing the most significant function. Proteins in bold fond are part of a protein cluster identified by TAC analysis. **b)** The 3 most significant pathways identified are listed with the associated proteins. **c)** 22 of the 38 proteins are connected in an interaction network. Green= MAM/sham expression ratio<1. Red= MAM/sham expression ratio>1. Mixed colors= subunits/isoforms differentially expressed. Non-coloured

symbols=not significant in LC-MS^E analysis, although incorporated as an interacting protein by the IPKB software.

Figure 4. Multivariate and univariate analysis of full resolution ^{1}H-NMR spectral data of MAM and sham hippocampi. a) The scores plot of the PLS-DA model shows a sharp separation between MAM and the sham group (Q^2=0.62). **b)** Representative sample spectrum of a sham rat. The partially overlaying resonance regions of the 20 identified metabolites are indicated. **c)** The coefficients plot of the OPLS-DA analysis indicates significantly different metabolic profiles for MAM and sham animals (Q^2=0.35). Labeled spectral regions show metabolites contributing to the difference between the two groups. The direction of the peak indicates the direction of metabolite level differences (up= higher measurements in MAM rats, down=higher measurements in sham rats).The importance of the contribution to the difference between the groups are color-coded according the correlation coefficient heat map (red=high contribution, dark blue=low contribution). **d)** Univariate analysis of manually integrated ^{1}H-NMR spectral data. The table presents the non-overlapping metabolic resonance groups and the ratio of the signal means of MAM and sham rats. Analytes with a significant difference ($p<0.05$) of the integrated signal are highlighted.

Figure 5. MAM-treatment on E17 resulted in reduced synaptic transmission in transverse hippocampal slices. a) fEPSPs in sham slices are blocked by GYKI53784. **b)** fEPSPs in MAM slices are blocked by GYKI53784. **c)** fEPSPs in sham slices are unaffected by AP5. **d)** fEPSPs in MAM slices are unaffected by AP5. Scale bar for a) and c) (sham traces) represents 0.5 mV and 20 ms. Scale bar for b) and d) (MAM traces) represents 0.3 mV and 20 ms. **e)** Example traces at increasing stimulation strengths showing FVs (the first fast peak) and fEPSPs (the second slow peak). Scale bars represent 1 mV and 20 ms. **f)** Comparison of the FV and the fEPSP in MAM (filled points) and sham (open points) hippocampal slices. **g)** Linear regression analysis of input output relation from Figure 5f.

TITLES AND LEGENDS TO TABLES

Table 1. Differentially expressed candidate proteins in hippocampal tissue derived from MAM and sham rats. The table shows the proteins in **a)** fraction 1 (10 MAM and 10 sham rats) and **b)** fraction 2 (10 MAM and 10 sham rats) indicating averaged protein intensities (rounded to integers) and the standard deviation (SD), MAM/sham protein abundance ratios, p-values and relative standard deviation (RSD) for the measurement of each protein (determined by analysis of 5 quality controls which have been prepared and analyzed with the MAM and sham samples).

a)

PROTEIN	Spiked concetration (ng/µl) group A	group B	Ratio expected	Ratio measured	Deviation of ratio
Albumin (porcine)	1	1	1	0.80	20%
Asialofetuine (bovine)	1	3	0.33	0.34	3%
Lactogen (human)	2	3	0.66	0.55	17%
Casein β (bovine)	4	2	0.5	0.31	39%

b)

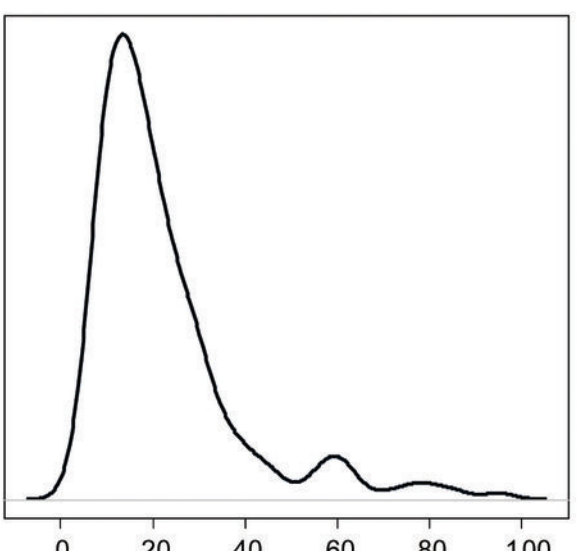

c)

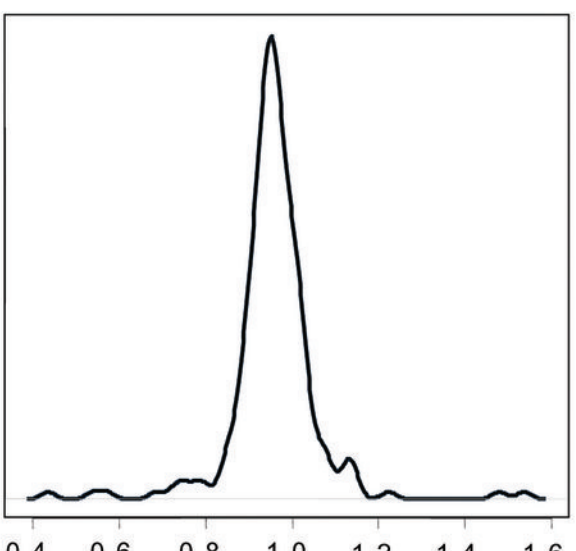

a)

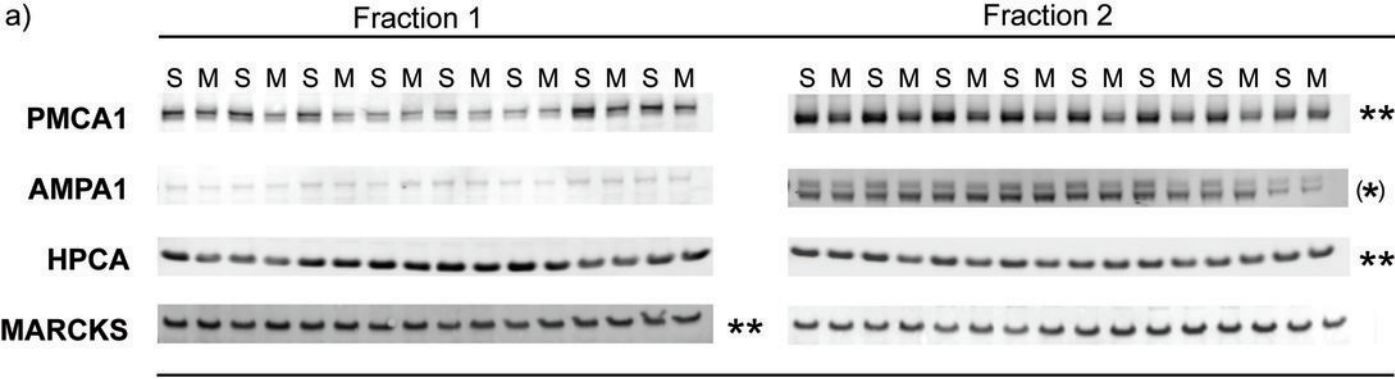

M MAM sample S SHAM sample * p<0.05 ** p<0.01 (*) p<0.01 for ratio of phosphorylated and unphosporylated form

b)

PROTEIN	LC-MS Fraction 1 Ratio MAM/SHAM	LC-MS Fraction 1 p-value	LC-MS Fraction 2 Ratio MAM/SHAM	LC-MS Fraction 2 p-value	IMMUNOBLOT Fraction 1 Ratio MAM/SHAM	IMMUNOBLOT Fraction 1 p-value	IMMUNOBLOT Fraction 2 Ratio MAM/SHAM	IMMUNOBLOT Fraction 2 p-value	Correlation LC-MS/WB[1]
PMCA1	0.86	0.292	0.86	2.17×10^{-7}	0.68	0.107	0.75	0.006	0.7**
AMPA1	-	-	0.93	1.46×10^{-4}	-	-	0.90|1.00	0.108|0.99	0.46|0.21*
ARP3	1.04	0.410	0.89	3.00×10^{-4}	0.99	0.930	0.92	0.313	0.37
HPCA	0.81	5.76×10^{-6}	0.85	3.27×10^{-4}	0.86	0.275	0.87	0.009	0.63*
SYNJ1	-	-	0.93	5.51×10^{-4}	1.05	0.688	0.94	0.743	0.08
MARCKS	1.21	1.44×10^{-4}	1.18	2.18×10^{-4}	1.13	0.006	1.05	0.691	0.39

[1] Spearman correlation coefficent of LC-MS^E and immunoblot measurements , significance of correlation is indicated as ** p<0.01 * p<0.05

c)

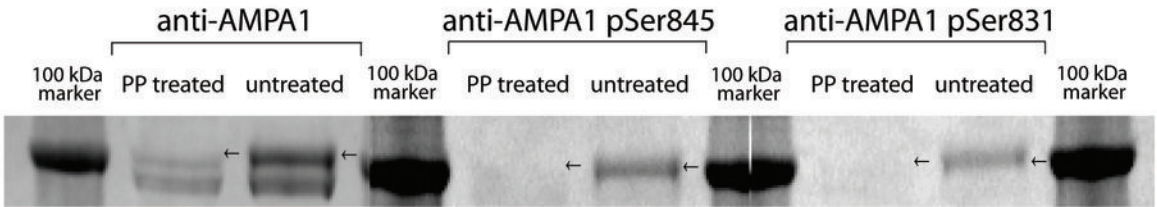

a) FUNCTIONAL ANALYSIS

CELL-TO-CELL SIGNALING AND NERVOUS SYSTEM FUNCTION	
Predominantly processes of synaptic transmission and plasticity Significance of functional associations: Fisher's exact test $p=4.05x10^{-7}$ - $4.47x10^{-2}$	Actin-related protein 3 (ACTR3), amphiphysin (AMPH), Na+/K+ transporting ATPase (ATP1A1), **Ca2+ transporting ATPase (PMCA1)** basigin (BSG), voltage-dependent calcium channel (CACNG8), calcium/calmodulin-dependent protein kinases (CAMK2A, CAMK2D, CAMK2G), dynamin 1 (DNM1), FK506 binding protein 1A (FKBP1A), glutaminase (GLS), **glutamate receptors AMPA (AMPA1, AMPA2)**, myosin (MYH4), neural cell adhesion molecule 1 (NCAM1), **protein phosphatase 3 (PPP3CA)**, peroxiredoxin 6 (PRDX6), RAB14 protein (RAB14), glial high affinity glutamate transporter (SLC1A3), synaptic vesicle glycoprotein 2B (SV2B), **synaptojanin 1 (SYNJ1)**, tubulin (TUBA8)

b) PATHWAY ANALYSIS

CALCIUM SIGNALING Fisher's exact test Fisher's exact test $p= 9.34x10^{-9}$	**AMPA1, AMPA2**, CAMK2A, CAMK2D, CAMK2G, **PMCA1** , MYH4, **PPP3CA**
LONG TERM POTENTIATION Fisher's exact test Fisher's exact test $p= 2.65x10^{-7}$	AMPA1, AMPA2, CAMK2A, CAMK2D, CAMK2G, **PPP3CA**
GLUTAMATE RECEPTOR SIGNALING Fisher's exact test Fisher's exact test $p= 1.19x10^{-5}$	GLS, **AMPA1, AMPA2,** MYH4, **PPP3CA,** SLC1A3

c) NETWORK ANALYSIS

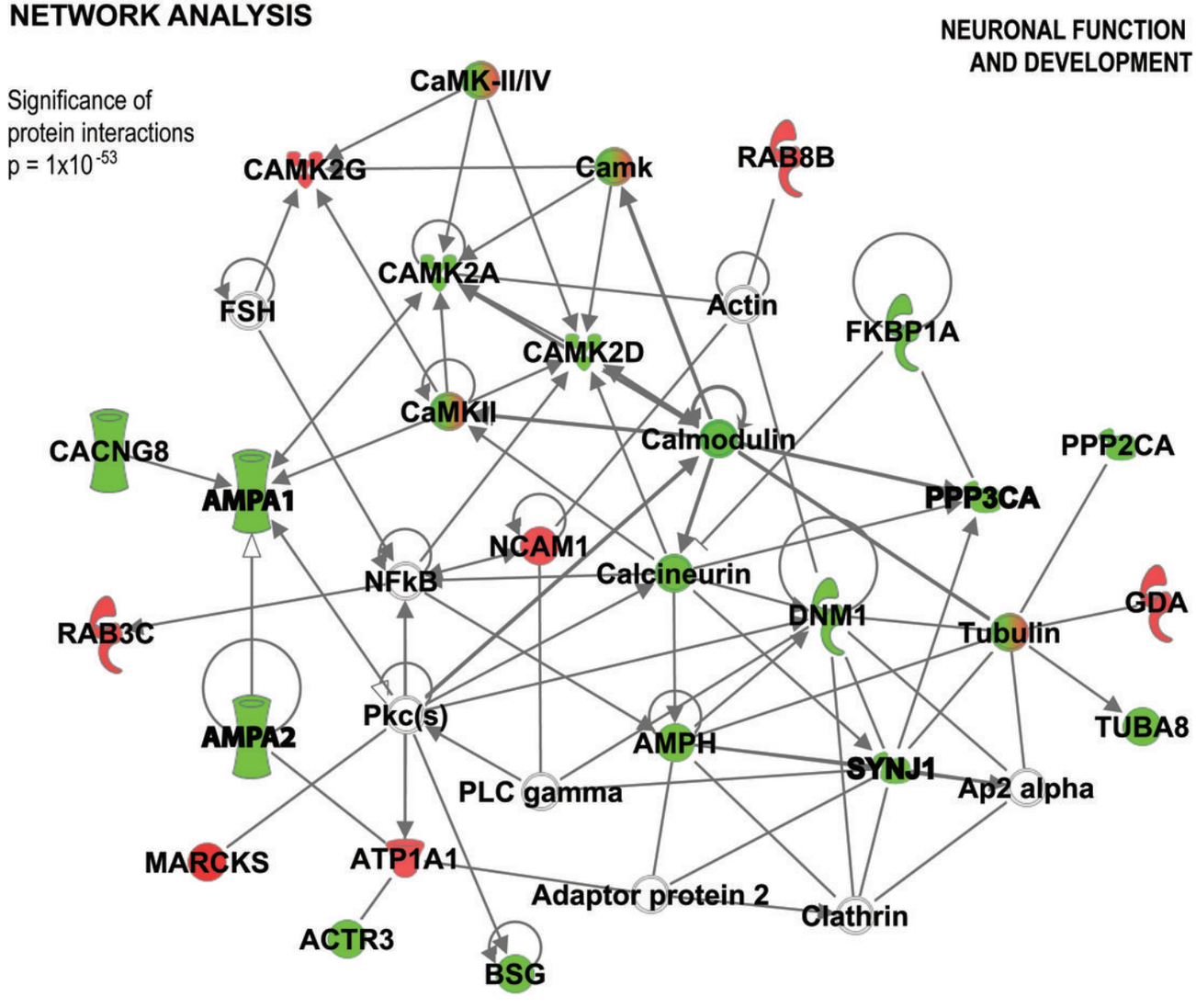

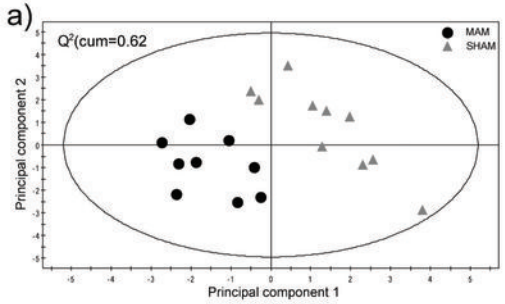

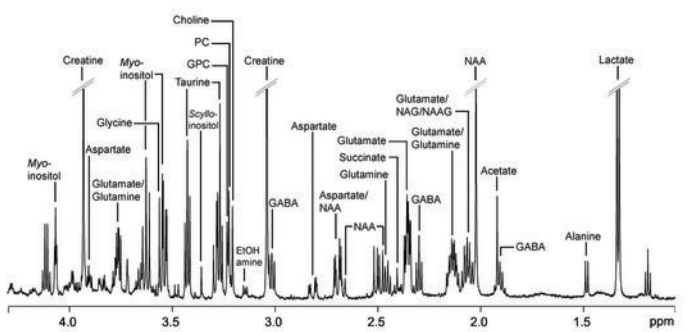

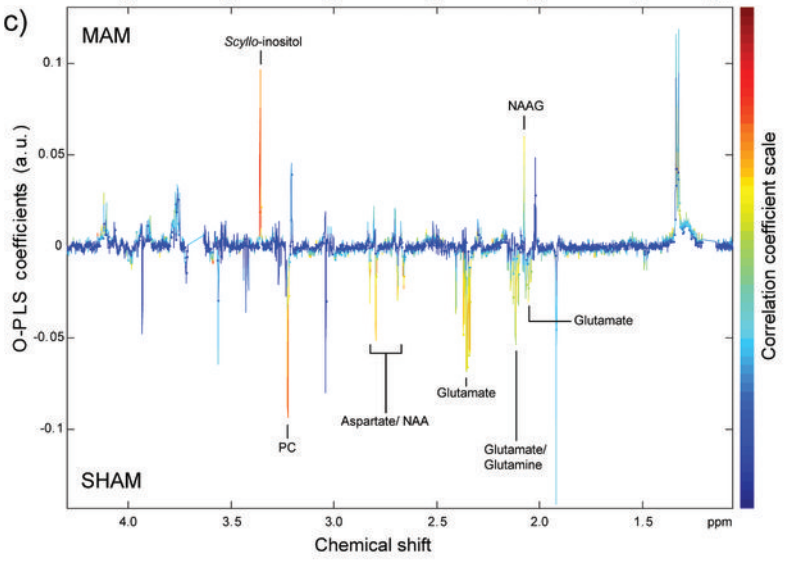

d)

Metabolite group		Ratio MAM/SHAM		p-value*
chemical shift (ppm)				
Acetate		1.92	0.81	0.0751
Alanine		**1.50**	**0.91**	**0.0027**
Aspartate		2.81	0.89	0.1039
Choline		3.21	1.07	0.3119
Creatine	(1)	3.94	0.98	0.4393
	(2)	3.04	0.98	0.2458
Ethanolamine		3.15	0.99	0.8627
GABA		2.3	1.01	0.6749
Glutamate	**(1)**	**2.06**	**0.90**	**0.0004**
	(2)	**2.35**	**0.95**	**0.0178**
Glutamine		**2.14**	**0.94**	**0.0009**
Glycine		**3.57**	**0.88**	**0.0218**
GPC		3.23	0.91	0.4053
Lactate	(1)	4.12	1.05	0.2371
	(2)	1.33	1.04	0.1490
Myo-inositol	(1)	4.06	0.99	0.6396
	(2)	3.54	1.00	0.8395
NAA		2.02	1.00	0.9915
Phosphocholine		**3.22**	**0.84**	**0.0013**
Scyllo-inositol		**3.35**	**1.61**	**0.0060**
Succinate		2.41	0.85	0.0532
Taurin		3.42	0.97	0.2118

* t-test

a)

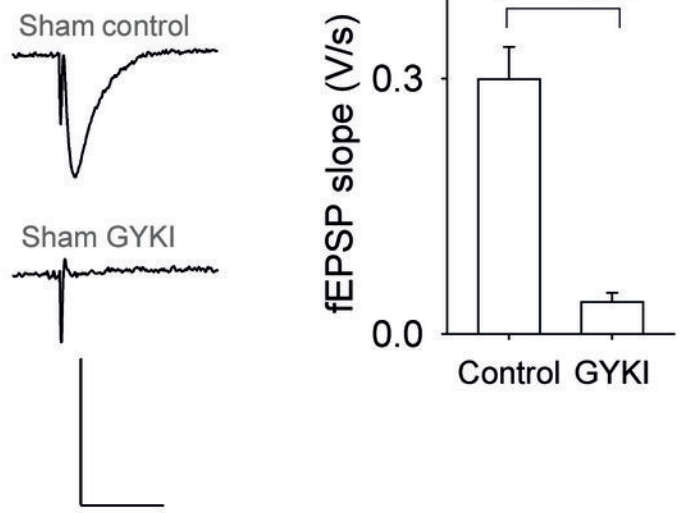
Sham control
Sham GYKI
P < 0.05
fEPSP slope (V/s)
0.3
0.0
Control GYKI

b)

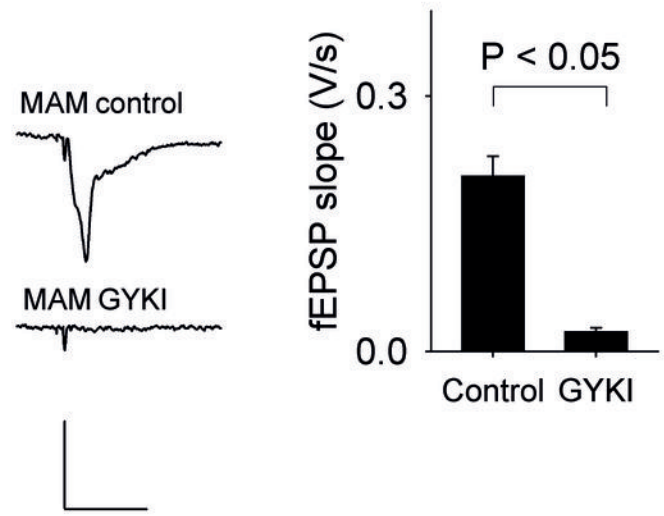
MAM control
MAM GYKI
P < 0.05
fEPSP slope (V/s)
0.3
0.0
Control GYKI

c)

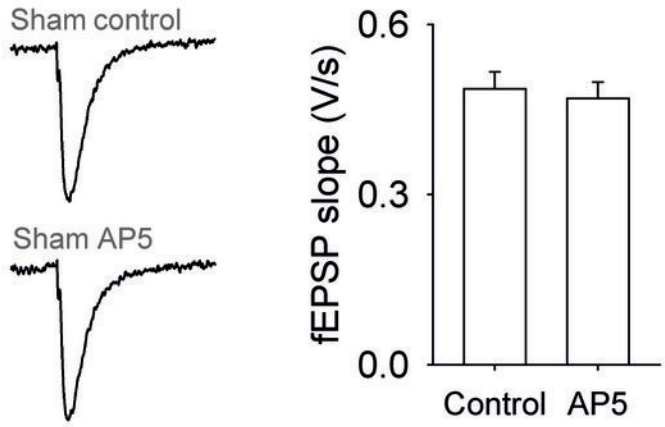
Sham control
Sham AP5
fEPSP slope (V/s)
0.6
0.3
0.0
Control AP5

d)

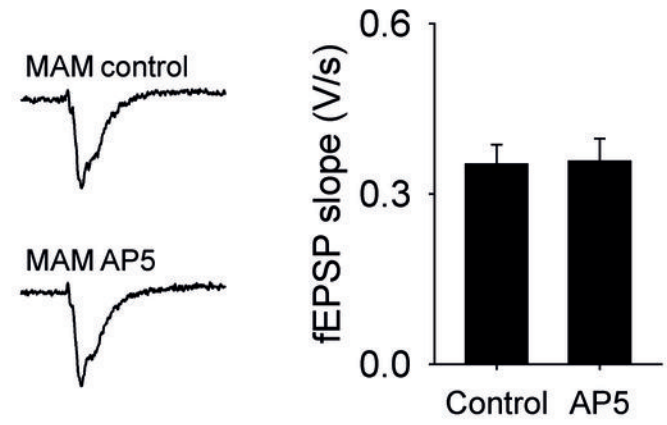
MAM control
MAM AP5
fEPSP slope (V/s)
0.6
0.3
0.0
Control AP5

e)

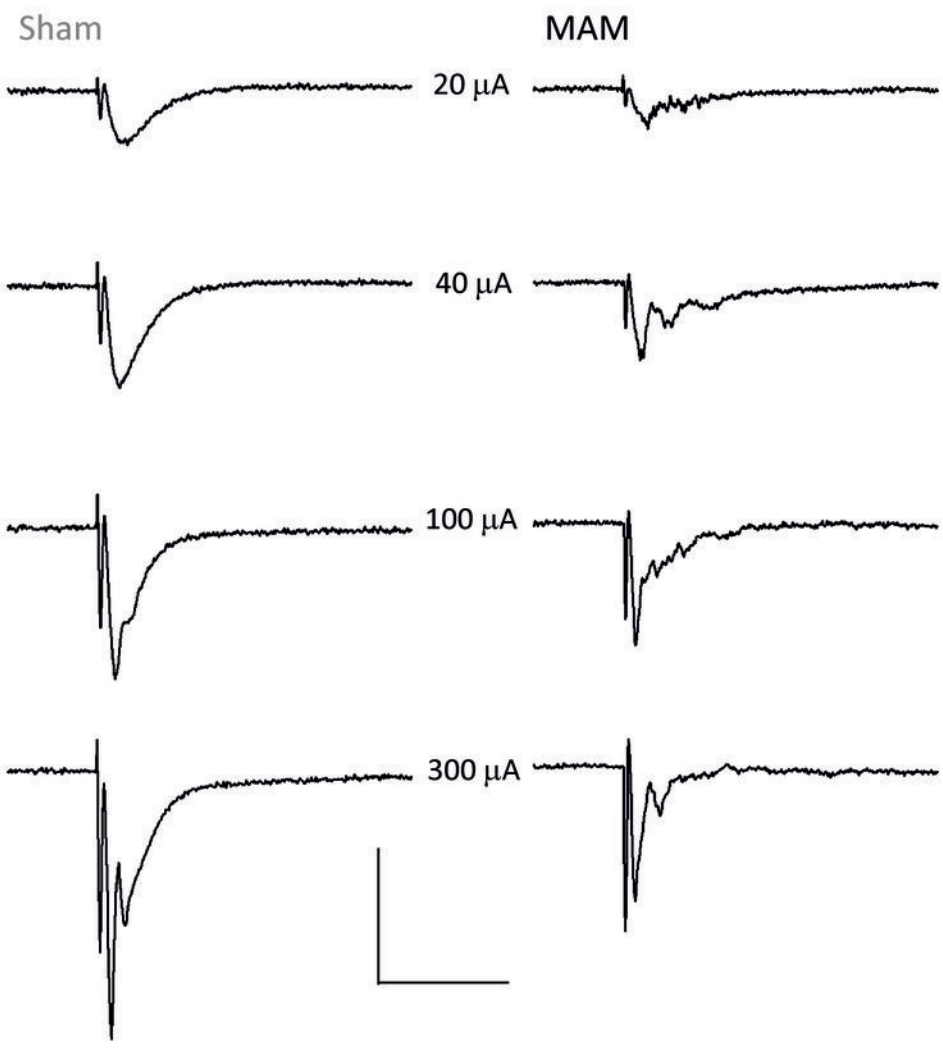
Sham
MAM
20 μA
40 μA
100 μA
300 μA

f)

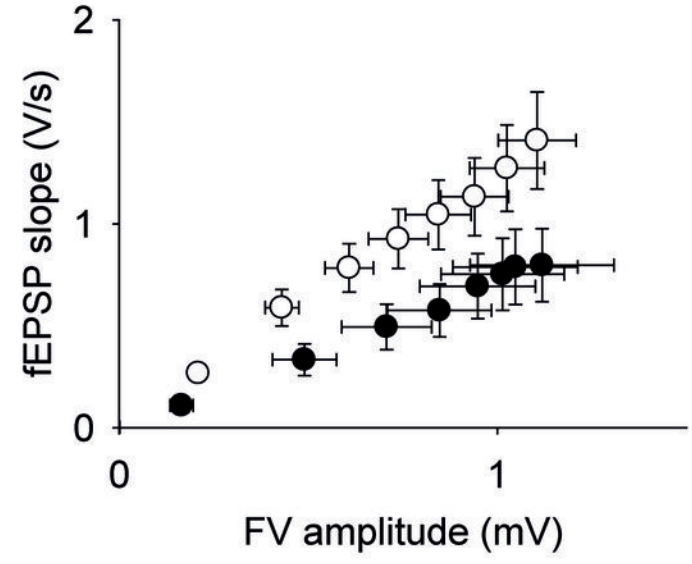
fEPSP slope (V/s)
2
1
0
0
1
FV amplitude (mV)

g)

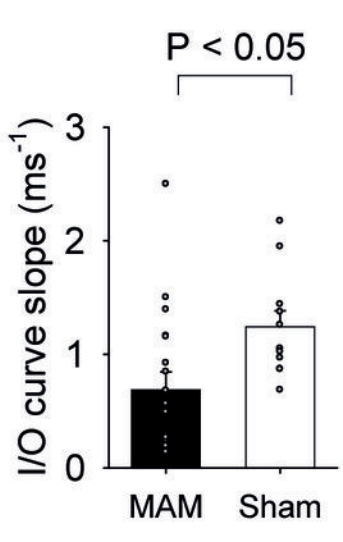
P < 0.05
I/O curve slope (ms-1)
3
2
1
0
MAM
Sham

a)

PROTEINS FRACTION 1	SwissProt ID	Gene name	Peptides quantified	Sequence coverage [%]	Average intensity MAM ± SD	Average intensity SHAM ± SD	Ratio MAM/SHAM	p-value	RSD QCs [%]
Guanine deaminase	Q9WTT6	GDA	41	76	31338 ± 1839	28491 ± 1490	1.09	0.0027	1
Hippocalcin	P84076	HPCA	21	86	49947 ± 4522	62606 ± 2655	0.80	0.0000	8
Lactate dehydrogenase A	P04642	LDHA	40	89	85713 ± 5698	94515 ± 6680	0.91	0.0058	3
Myristoylated alanine rich protein kinase C substrate	P30009	MARCKS	13	60	24461 ± 1511	19924 ± 2094	1.21	0.0001	2

b)

PROTEIN FRACTION 2	SwissProt ID	Gene name	Peptides quantified	Sequence coverage [%]	Average intensity MAM ± SD	Average intensity SHAM ± SD	Ratio MAM/SHAM	p-value	RSD QCs [%]
Amphiphysin	O08838	AMPH	22	49	19898 ± 1111	21274 ± 1369	0.94	0.0244	2
ARP3 actin-related protein 3	Q4V7C7	ACTR3	25	70	24523 ± 837	27415 ± 1753	0.89	0.0003	8
ATPase, Ca++ transporting, plasma membrane 1	P11505	PMCA1	69	62	26650 ± 990	31272 ± 1463	0.85	0.0000	3
ATPase, Na+/K+ transporting	P06685	ATP1A1	60	51	81921 ± 4513	77393 ± 4361	1.06	0.0342	2
Basigin	P26453	BSG	8	30	10443 ± 1056	12180 ± 830	0.86	0.0014	12
Calcium channel, voltage-dependent, gamma subunit 8	Q8VHW5	CACNG8	3	14	20737 ± 2923	24053 ± 2917	0.86	0.0188	7
Calcium/calmodulin-dependent protein kinase II alpha	P11275	CAMK2A	31	65	107485 ± 10925	127287 ± 11068	0.84	0.0010	6
Calcium/calmodulin-dependent protein kinase II delta	P15791	CAMK2D	17	44	18553 ± 1273	20051 ± 1139	0.93	0.0138	6
Calcium/calmodulin-dependent protein kinase II gamma	P11730	CAMK2G	17	47	12968 ± 670	11998 ± 695	1.08	0.0058	7
Calmodulin	P62161	CAM	17	89	97711 ± 12227	109183 ± 6598	0.89	0.0257	9
Capping protein (actin filament) muscle Z-line, alpha 2	Q3T1K5	CAPZA2	8	42	16601 ± 837	18153 ± 1505	0.91	0.0124	7

Dipeptidyl-peptidase 6	P46101	DPP6	13	26	16133 ± 770	17054 ± 722	0.95	0.0118	7
Dynamin 1	P21575	DNM1	73	81	37638 ± 1047	39025 ± 1555	0.96	0.0313	2
FK506 binding protein 1A, 12kDa	Q62658	FKBP1A	7	78	30458 ± 3165	36348 ± 2870	0.84	0.0009	7
Glial high affinity glutamate transporter member 3	P24942	SLC1A3	21	46	61487 ± 3811	57770 ± 3472	1.06	0.0335	6
Glutamate receptor, ionotropic, AMPA 1	P19490	AMPA1	27	42	14177 ± 870	15938 ± 659	0.89	0.0001	7
Glutamate receptor, ionotropic, AMPA 2	P19491	AMPA2	52	62	13719 ± 588	14760 ± 888	0.93	0.0064	6
Glutaminase	P13264	GLS	46	70	22286 ± 1140	24418 ± 1362	0.91	0.0013	5
Hemoglobin, beta	P02091	HBB	15	83	87376 ± 20210	69534 ± 12326	1.26	0.0217	10
Hippocalcin	P84076	HPCA	15	70	32618 ± 2910	38319 ± 2639	0.85	0.0003	9
Hydroxyprostaglandin dehydrogenase 15-(NAD)	O08699	HPGD	5	32	14214 ± 853	15848 ± 1917	0.90	0.0354	5
Limbic system-associated membrane protein	Q62813	LSAMP	4	9	11014 ± 1105	12013 ± 659	0.92	0.0231	12
Myosin, heavy chain 4	Q29RW1	MYH4	27	20	16105 ± 510	16803 ± 555	0.96	0.0093	6
Myristoylated alanine rich protein kinase C substrate	P30009	MARCKS	16	63	18180 ± 954	14564 ± 3383	1.25	0.0218	9
Neural cell adhesion molecule 1	P13596	NCAM1	46	66	33399 ± 1662	30806 ± 1661	1.08	0.0029	5
Peroxiredoxin 6	O35244	PRDX6	20	74	22516 ± 1223	20572 ± 2199	1.09	0.0294	9
Protein phosphatase 2, catalytic subunit, alpha isoform	P63331	PPP2CA	3	21	4523 ± 815	5932 ± 1049	0.76	0.0033	29
Protein phosphatase 3, catalytic subunit, alpha isoform	P63329	PPP3CA	31	66	37842 ± 1688	41973 ± 3455	0.90	0.0042	5
RAB14	P61107	RAB14	23	74	19017 ± 1391	20161 ± 707	0.94	0.0382	9
RAB3C	P62824	RAB3C	12	49	40694 ± 3487	36178 ± 3076	1.12	0.0076	6
RAB8B	P70550	RAB8B	7	51	11284 ± 837	10442 ± 851	1.08	0.0393	11
Solute carrier family 4, sodium bicarbonate cotransporter, member 4	Q9JI66	SLC4A4	18	29	11815 ± 832	11013 ± 650	1.07	0.0286	4

Synaptic vesicle glycoprotein 2B	Q63564	SV2B	3	8	11568 ± 1315	13008 ± 1322	0.89	0.0261	17
Synaptojanin 1	Q62910	SYNJ1	33	27	26469 ± 1194	29115 ± 1604	0.91	0.0006	4
Tubulin, alpha 8	Q6AY56	TUBA8	12	36	14945 ± 2221	17439 ± 1984	0.86	0.0268	10
Tubulin, beta 2B	Q3KRE8	TUBB2B	4	16	22304 ± 1794	20001 ± 2580	1.12	0.0331	5